A Solid-State ^{93}Nb and ^{19}F NMR Spectroscopy and X-ray Diffraction Study of Potassium Heptafluoroniobate(V): Characterization of ^{93}Nb, ^{19}F Coupling, and Fluorine Motion

Lin-Shu Du, Robert W. Schurko,† Kwang Hun Lim, and Clare P. Grey*

Department of Chemistry, State University of New York at Stony Brook, Stony Brook, New York, 11794-3400

Received: September 11, 2000; In Final Form: November 13, 2000

A variety of NMR interactions have been characterized by solid-state NMR spectroscopy in potassium heptafluoroniobate, K_2NbF_7, which contains fluorine atoms arranged about a central niobium atom in a heptacoordinate, capped trigonal prism arrangement. Simulations of ^{93}Nb MAS NMR spectra acquired at 11.7 T and at high spinning speeds (35 kHz) yielded the nuclear quadrupole coupling constant, $C_Q(^{93}Nb)$, the asymmetry parameter, η, and the isotropic chemical shift, δ_{iso}. From the analysis of ^{93}Nb NMR spectra of stationary samples of K_2NbF_7, the niobium chemical shielding anisotropy (span, $\Omega = 200$ ppm) and the relative orientation of the electric field gradient (EFG) and chemical shielding (CS) tensors were determined. The ^{93}Nb MAS NMR spectra acquired at lower spinning speeds, where the spinning sidebands are not separated from the centerband, were also simulated by using an efficient time propagation algorithm based on Floquet theory. The $C_Q(^{93}Nb)$ is seen to increase with decreasing temperature, varying from 29 to 40 MHz from 150 to 0 °C, respectively, with the following parameters determined at room temperature: $C_Q = 38.5(2)$ MHz, $\eta = 0.35(2)$, and $\delta_{iso} = -1600(5)$ ppm. Slightly distorted ten-peak multiplets are observed in the solid-state ^{19}F MAS NMR spectra, which arise from *J*-coupling and residual dipolar coupling between the ^{19}F and ^{93}Nb nuclei. Simulations of the ^{19}F MAS NMR spectra yield values of $^1J(^{93}Nb,^{19}F) = 204(2)$ Hz and $\delta_{iso}(^{19}F) = 76.28(2)$ ppm. Variable-temperature ^{19}F MAS NMR experiments demonstrate that intramolecular fluorine motion becomes significant above −100 °C resulting in a reduction in the fluorine second moments and the ^{93}Nb, ^{19}F dipolar couplings. An irreversible phase transition is observed at ca. 160 °C by ^{19}F and ^{93}Nb NMR, as well as by time-resolved synchrotron X-ray powder diffraction techniques.

Introduction

Potassium heptafluoroniobate has been widely studied, primarily due to its use as a low melting electrolyte in niobium electrodeposition processes.[1] K_2NbF_7, and its isostructural compound K_2TaF_7, have also been investigated for their luminescent properties.[2] Potassium heptafluoroniobate(V) represents an example of a transition metal compound with the metal atom in a heptacoordinate environment, the arrangement of fluorine atoms around the metal forming a capped trigonal prism (Figure 1). Since very little information is known regarding the chemical shielding (CS) and electric field gradient (EFG) tensors in seven-coordinate environments, it represents an interesting model compound for NMR studies. The analogous compounds, K_3ZrF_7, and isostructural K_2TaF_7, have previously been studied with a combination of X-ray diffraction, IR, Raman, and second-moment analysis of wide-line ^{19}F NMR data.[3] These complexes exhibit considerable intraionic fluorine motion above 150 K, involving rearrangement of the fluorine atoms about the metal centers. In the case of K_2TaF_7, the anion has been described as undergoing "floppy reorientations" on the NMR time scale.[3]

The crystal structure of K_2NbF_7 has been previously determined by both X-ray[4] and neutron diffraction[5] techniques. The NbF_7^{2-} anion has C_1 symmetry, but there is an approximate mirror plane containing the F7 atom (see Figure 1). The anion is surrounded by a cage of ten K^+ cations, with atoms F1 through F4 possessing three nearest neighbor K^+ ions, and atoms F5 through F7 having only two nearest K^+ neighbors. The molecule possesses a variety of Nb−F bond distances (1.926 to 1.971 Å), F−Nb−F bond angles (73.9 to 97.7°), and

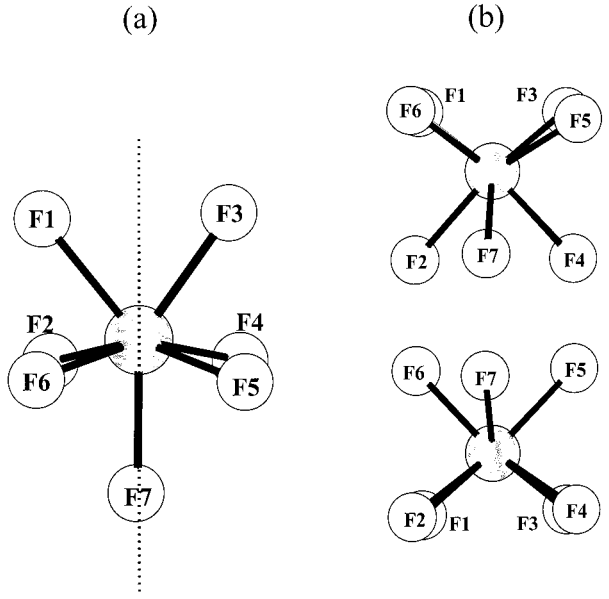

Figure 1. Potassium heptafluoroniobate(V) (a) pictured along the approximate mirror plane and (b) two alternative perspectives obtained by rotating the molecule through this approximate mirror plane.

* Author to whom correspondence should be addressed: Phone: 631-632-9548. Fax: 631-632-5731. E-mail: cgrey@notes.cc.sunysb.edu.

† Current address: Department of Chemistry and Biochemistry, School of Physical Sciences, University of Windsor, Windsor, Ontario, Canada N9B 3P4.

10.1021/jp0032006 CCC: $20.00
Published on Web 01/10/2001

intraionic F−F distances (2.357 to 2.912 Å). Neutron diffraction studies indicate that the niobium atom undergoes some degree of isotropic thermal motion.[5] F5 and F6 were observed to have large displacements perpendicular to the Nb−F bond axes (as indicated by large thermal ellipsoids), which are thought to be the result of the particular arrangement of the surrounding potassium ions.

^{93}Nb, ^{19}F indirect spin−spin coupling (*J*-coupling), ^{93}Nb, ^{19}F and ^{19}F, ^{19}F direct dipolar coupling, the ^{93}Nb quadrupolar interaction, and ^{93}Nb chemical shielding anisotropy (CSA) are all probed in this paper with ^{93}Nb and ^{19}F solid-state NMR, to characterize the local structure around the niobium atoms and to determine how this varies with temperature. The temperature of the phase transition observed in this compound, which has been briefly discussed in the literature,[6] is investigated by using time-resolved X-ray diffraction.

Both ^{93}Nb (spin-9/2) and ^{19}F (spin-1/2) are 100% naturally abundant isotopes with large magnetogyric ratios. The niobium nuclear quadrupole moment, eQ, is relatively large ($Q(^{93}\text{Nb}) = -0.22$ H 10^{-28} m^2);[7] thus, ^{93}Nb spectra are dominated by the quadrupolar interaction and the resonance from the central transition ($|-1/2\rangle \rightarrow |1/2\rangle$) may be extremely broad. A combination of ^{93}Nb NMR spectra, acquired at multiple fields on stationary samples and under conditions of fast MAS frequencies, were required in this work in order to extract the ^{93}Nb quadrupole coupling constant (C_Q), the quadrupolar asymmetry parameter, η, and the ^{93}Nb isotropic chemical shift and CSA. In this paper, the principal components of the EFG tensor are defined as $|V_{33}| \geq |V_{22}| \geq |V_{11}|$, where $C_Q = eQV_{33}/h$, and $\eta = (V_{11} - V_{22})/V_{33}$.

Determination of the chemical shift anisotropy of quadrupolar nuclei with large values of C_Q requires careful simulation of the experimental static spectrum of the central transition. The line shape of this resonance is dependent upon the quadrupolar parameters, the CS tensor, and the relative orientation of the CS and EFG tensors. The dipolar interaction tensor may also have to be considered if it is of appreciable magnitude in comparison to the chemical shielding and quadrupolar interactions. Since the problem of simulating such NMR spectra has been considered in great detail for nuclei such as ^{87}Rb (spin 3/2) and ^{133}Cs (spin 7/2), and is well understood,[8−12] the theory underlying the treatment of the problem is not described here. Nonetheless, a general analytical equation describing the appearance of the static spectrum of the central transition of the quadrupolar nucleus with dominant quadrupolar and anisotropic chemical shielding interactions can be written as

$$\nu_{1/2\leftrightarrow -1/2} = \nu_0 + \nu_Q^{(2)}(\theta,\phi) - \nu_{CS}(\theta,\phi,\alpha,\beta,\gamma) \qquad (1)$$

where ν_0 is the Larmor frequency of the quadrupolar nucleus and θ and ϕ are polar and azimuthal angles, respectively, which describe the orientation of the EFG tensor with respect to the applied magnetic field, and α, β, and γ are Euler angles which define the orientation of the CS tensor with respect to the EFG tensor via the following rotational operations:[13]

$$R(\alpha,\beta,\gamma) = R_{z''}(\gamma)\, R_{y'}(\beta)\, R_z(\alpha) \qquad (2)$$

Explicit expressions for $\nu_Q^{(2)}$ and ν_{CS} are given elsewhere.[11]

Fluorine-19 MAS experiments were used to measure the one-bond indirect spin−spin coupling, $^1J(^{93}\text{Nb},^{19}\text{F})$, in solid K_2NbF_7. *J*-couplings would normally be unobservable in the ^{19}F MAS NMR spectra due to line broadening caused by the large fluorine homonuclear dipolar couplings; however, our previous experiments on both α- and β-PbF_2 have shown that direct, one-bond couplings may sometimes be observed when fast MAS frequencies are used.[14] Measurements of *J*-coupling constants in the type of spin pairs under study here are usually not accessible via solution-state NMR experiments, owing to the rapid, quadrupole-dominated spin−lattice relaxation of the quadrupolar nucleus, and corresponding scalar relaxation of the second kind at the spin-coupled spin-1/2 nucleus.[15] Normally, the spin-1/2 NMR resonances are broadened in these cases, such that the fine-structure resulting from *J*-coupling is not observable, particularly for a quadrupolar nucleus with a large quadrupole moment. It is, however, possible to measure *J*-couplings from the spin-1/2 spectra if the coupled quadrupolar nucleus exists within a symmetric environment, which results in reduced values of C_Q, and longer spin−lattice relaxation times for the quadrupolar nucleus.

The spacings between peaks in the multiplet arising from *J*-coupling will be affected by residual dipolar coupling between the spin-1/2 and quadrupolar nuclei. This is a well-documented phenomenon, and has been observed for a wide variety of spin pairs.[16−18] Residual dipolar coupling arises from the presence of nonzero *C* and *D* terms in the dipolar "alphabet" Hamiltonian, which cannot be averaged by MAS. These terms arise because the eigenstates of the quadrupolar nucleus are not quantized in the direction of the static magnetic field, but rather must be described by linear combinations of the pure Zeeman states of the quadrupolar nucleus. This residual dipolar coupling manifests itself in the MAS spectrum as an increasing or decreasing spacing between the peaks in the multiplet.

First-order perturbation theory[19−21] and full diagonalization of the combined Zeeman and quadrupolar Hamiltonians[22,23] have been utilized in the treatment of this problem. The former treatment is used for simulations of the ^{19}F MAS NMR spectra in this paper, and is valid in the limit where $C_Q/(4S\,(2S-1)) \ll \nu_0$, where ν_0 is the Larmor frequency of the quadrupolar nucleus. The frequencies of each of the peaks in the multiplet are shifted from the isotropic chemical shift by both the *J*-coupling interaction and the residual dipolar shift, as given by

$$\nu_{m_s} = \nu_{iso} - m_s J_{iso} + \frac{S(S+1) - 3m_s^2}{S(2S-1)} d \qquad (3)$$

where ν_{m_s} is the frequency of a peak in the spin-1/2 multiplet corresponding to the spin state, m_S, of the quadrupolar nucleus, ν_{iso} is the isotropic frequency, S is the spin of the quadrupolar nucleus, and d is the residual dipolar shift, which can be written as

$$d = \left[\frac{3C_Q R_{eff}}{20\nu_0}\right][(3\cos^2\beta^D - 1) + \eta\sin^2\beta^D\cos 2\alpha^D] \qquad (4)$$

Here, R_{eff} is the effective dipolar coupling constant, given by $R_{eff} = R_{DD} - \Delta J/3$, where R_{DD} is the dipolar coupling constant ($R_{DD} = (\mu_0/4\pi)(\gamma_I\gamma_S\hbar/2\pi)r_{IS}^{-3}$) and ΔJ is the anisotropy in the **J**-tensor ($\Delta J = J_{||} - J_\perp$). The **J** tensor is presumed to be axially symmetric within unique axes directed along the bond vector.[24] The angles β^D and α^D are the polar and azimuthal angles that describe the orientation of the dipolar vector with respect to the EFG tensor. The isotropic *J*-coupling can be measured from the splittings between the central peaks of the multiplet, which result from coupling to the +1/2 and −1/2 spin states of the niobium nucleus. As seen from eq 4, an increase in C_Q or R_{eff}, or a decrease in the Larmor frequency, results in increased residual dipolar couplings.

Experimental Section

Potassium heptafluoroniobate was obtained from Aldrich and used without further purification. Samples were powdered and packed into 2.5, 3.2, and 7.5 mm o.d. ZrO_2 rotors. Solid-state ^{19}F and ^{93}Nb NMR spectra were obtained with wide-bore CMX-360 (8.5 T) and Bruker AMX-500 (11.7 T) spectrometers at operating frequencies of 338.75 and 470.08 MHz, respectively, for ^{19}F, and of 87.96 and 122.06 MHz, respectively, for ^{93}Nb. Fluorine and niobium chemical shifts are referenced to neat $CFCl_3$ and $NbCl_5$ in CH_3CN, respectively, which are both set to 0.0 ppm. A Chemagnetics 3.2 mm double-resonance probe capable of reaching spinning frequencies, υ_{rot}, of 24 kHz was used on the CMX-360 spectrometer for the acquisition of ^{19}F and ^{93}Nb MAS spectra. A Chemagnetics 7.5 mm triple-resonance probe was used for acquiring ^{93}Nb spectra of stationary samples at 8.5 T. For all of the spectra collected with the Bruker AMX-500, a Bruker 2.5 mm triple-resonance probe capable of reaching spinning frequencies of 35 kHz was used. Room temperature ^{19}F MAS spectra were acquired at 8.5 T using single-pulse experiments with spinning frequencies of ca. 20 kHz, pulse widths of 2.4 μs, and pulse delays of 3 s, with collection of 5120 transients. At 11.7 T, single-pulse ^{19}F MAS experiments were conducted with spinning frequencies between 30 and 35 kHz, pulse widths of 4 μs, and pulse delays of 4 s, with ca. 160 scans for each experiment. Variable-temperature ^{19}F MAS spectra were acquired at 8.5 T with spinning frequencies of 17 kHz (measured temperature range: -150 to -50 °C) and 22 kHz (measured temperature range: -25 to 250 °C), which were chosen to ensure optimum spinning control of the sample during variable-temperature experiments. Hahn-echo ^{19}F experiments were performed in the measured temperature range from -150 to -50 °C, with pulse widths of 1.55 μs, pulse delays of 3 s, and 400 scans. Single-pulse ^{19}F experiments were performed from -25 to 250 °C, with pulse widths of 1.55 μs, pulse delays of 3 s, and collection of 60 transients.

The ^{93}Nb MAS and static spectra were obtained using Hahn-echo experiments at both fields. Niobium-93 MAS spectra were collected at 8.5 T using a 3.2 mm probe with rf fields of 120 kHz, with effective 90° pulse widths of 0.6 μs measured on actual solid sample ($\pi/10$ when measured with the solution standard), pulse delays of 0.5 s and acquisition of between 33 280 and 44 480 transients. Due to relatively long pulse rise times on the order of 0.2 to 0.4 μs, it was not possible to use any shorter pulses, to optimize the excitation of the entire central transition line shape. The ^{93}Nb static spectra at 8.5 T were collected using the 7.5 mm probe (for improved S/N) with rf field amplitudes of 74 kHz, pulse widths of 0.9 μs, pulse delays of 0.4 s, and collection of 20 000 transients. The ^{93}Nb spectra at 11.7 T were collected using a 2.5 mm probe with an rf field amplitude of 125 kHz, pulse widths of 0.4 and 1.0 μs, and pulse delays of 0.5 s with collection of 8190 and 65 536 transients for MAS and stationary samples, respectively.

The temperature inside the rotors was calibrated for the Chemagnetics probes, with $Pb(NO_3)_2$. The real temperature inside the rotor at a spinning speed of ca. 20 kHz, at "room temperature", when the temperature controller is not used, is actually 54 °C, due to frictional heating.[25] The experimentally determined relationship between the actual temperature in the rotors and the temperature measured by the thermocouple (external to the sample in the variable-temperature stack) is given by

$$Y = 8.41 + 1.08X \quad (5)$$

where X is the temperature set by the controller and Y is the real temperature. Unless stated explicitly, the measured temperature is given. No calibration data was available for the Bruker 2.5 mm probe, but an even larger difference between the real and measured temperature is expected. Static spectra were obtained with the 7.5 mm Chemagnetics probe, and even at the temperature extremes, errors of no more than ± 5 °C between the real and measured temperatures were determined.

The majority of ^{93}Nb and ^{19}F MAS NMR spectra were simulated using WSolids, which was developed by Dr. Klaus Eichele in Prof. Roderick E. Wasylishen's laboratory (Dalhousie University). WSolids utilizes the space-tiling algorithm of Alderman et al. for rapid generation of powder spectra.[26] The ^{93}Nb MAS spectra acquired at 8.5 T were simulated numerically by using an efficient time propagation algorithm based on Floquet theory.[27] Programs were written in the C++ programming language, using the GAMMA platform[28] for simulation of NMR spectra.

X-ray synchrotron powder diffraction data was collected at the beamline $\times$7B at the National Synchrotron Light Source, Brookhaven National Laboratory, with a Fuji imaging plate mounted perpendicular to the incoming beam. An external lanthanum hexaborate (LaB_6) standard was used to determine the wavelength ($\lambda = 0.9355$ Å). In situ high-temperature data were collected with a translating image plate camera built for time-resolved powder diffraction experiments.[29] K_2NbF_7 was packed in 0.5 mm quartz capillaries under nitrogen. Heating of the sample was synchronized with the horizontal movement of the image plate, allowing a series of powder patterns to be recorded. Slices of the powder data were extracted by integrating a 30 pixel (30 mm) wide vertical strip. The room temperature powder pattern was found to be consistent with the previously reported monoclinic structure of K_2NbF_7.[5]

Results

Niobium-93 MAS NMR. Niobium-93 MAS NMR spectra obtained under fast spinning conditions (i.e., $\nu_{rot} > 20$ kHz) at 8.5 and 11.7 T are shown in Figure 2. The spinning sidebands overlap with the central transition in the spectra acquired at the lower field (Figure 2a), making the determination of C_Q, η, and δ_{iso} from these spectra very difficult. However, examination of MAS spectra acquired at 11.7 T with a spinning speed of 35 kHz reveals that the sidebands are well separated, permitting analysis of the isotropic centerband. Simulations of the isotropic centerband yield values for C_Q, η, and δ_{iso} of 35.5(2) MHz, 0.35(2), and $-1600(10)$ ppm, respectively (Figures 2d and 2e). The fact that η is not near zero, which would indicate near-axial symmetry of the EFG tensor, is not surprising, given the asymmetric nature of the fluorine coordination about the niobium atom.

Simulation of the MAS spectra acquired at slower spinning speeds requires that the chemical shift anisotropy (CSA) and the relative orientation of the CSA and EFG tensors are considered, since both interactions play a role in determining the overall appearance of the spectra. The simulations are, therefore, dependent upon eight parameters: the quadrupolar parameters, C_Q and η, the three principal components of the chemical shift tensor (defined from least to most shielded, $\delta_{11} \geq \delta_{22} \geq \delta_{33}$), and three Euler angles defining the relative orientation of the CS and EFG tensors, α, β, and γ. Despite the large number of parameters, the simulations are, in theory, feasible, since C_Q and η can be independently determined from the high-speed MAS spectra. To perform these simulations, however, we used information concerning the CS tensor and the relative orientation of the CS and EFG tensors obtained from the analysis of static ^{93}Nb spectra discussed in the following

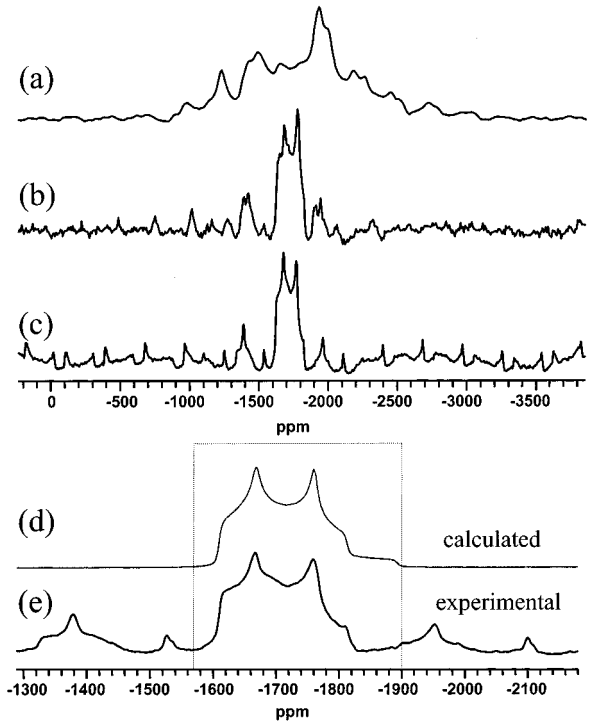

Figure 2. ^{93}Nb MAS NMR spectra of K_2NbF_7 at (a) 8.4 T, $\nu_{rot} = 23$ kHz, (b) 11.7 T, $\nu_{rot} = 32$ kHz and (c) 11.7 T, $\nu_{rot} = 35$ kHz. Expansions of the (d) calculated and (e) experimental isotropic centerbands of spectra acquired at 11.7 T, $\nu_{rot} = 35$ kHz. Simulation parameters: $C_Q = 35.5$ MHz, $\eta = 0.35$, and $\delta_{iso} = -1600$ ppm.

section. The parameters were then adjusted iteratively so that good fits of both the static and spinning spectra were obtained, with the same parameters. The only parameter that was allowed to vary between static and spinning spectra was C_Q due to the effect of spinning on the sample temperature and, thus, on C_Q. For reasons discussed below, a smaller value in comparison to the value used for the static spectra of 37.5 MHz was used for the simulations of the MAS spectra acquired at moderate spinning speeds, providing better agreement with experimental data.

Niobium-93 NMR Spectra of Stationary Samples: Niobium Chemical Shielding Anisotropy. Niobium-93 static NMR spectra acquired at 8.5 T with ^{19}F decoupling, and 11.7 T without ^{19}F decoupling, are presented in Figure 4. Simulated spectra are also shown, from which the following parameters have been determined: $C_Q = 38.5(2)$ MHz, $\eta = 0.35(2)$, and $\delta_{iso} = -1600(5)$ ppm. The span of the CS tensor, defined as $\Omega = \delta_{11} - \delta_{33}$, is 200(20) ppm. The skew of the CS tensor, $\kappa = 3(\delta_{22} - \delta_{iso})/\Omega$, where $-1 \leq \kappa \leq 1$, is equal to 0.0(2), indicating that the CS tensor is not axially symmetric.

The C_Q extracted from the static spectrum is larger than that observed by MAS NMR ($C_Q = 35.5$ MHz, with $\nu_{rot} = 35$ kHz). Simulations of static spectra acquired at both fields using $C_Q = 35.5$ MHz, resulted in calculated spectra which were significantly different from experimental results, even when the effects of niobium CSA were included. Careful analysis of a variety of different spectra acquired under different conditions suggested that the higher temperatures associated with fast MAS[30] were responsible for reducing the value of C_Q, and a series of variable-temperature ^{93}Nb experiments were performed to confirm this (see below).

The contribution of the niobium CSA to the ^{93}Nb spectra, which are largely dominated by the quadrupolar interaction, is relatively small. For instance, the contribution of CSA to the

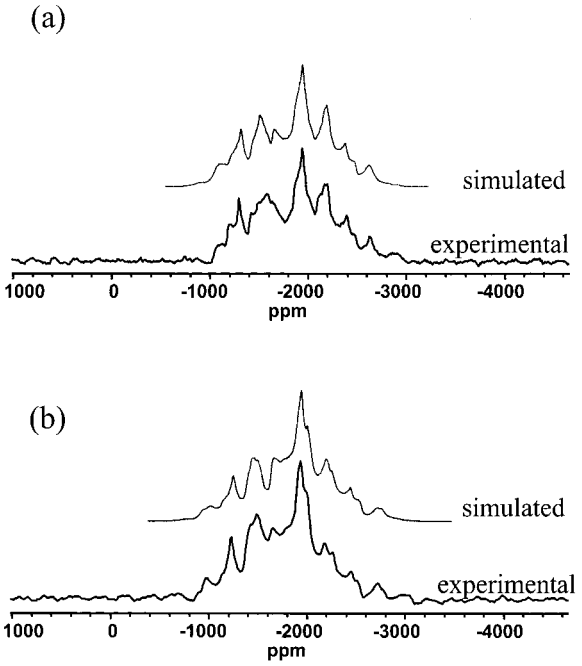

Figure 3. Experimental and simulated ^{93}Nb MAS NMR spectra of K_2NbF_7 acquired at 8.5 T at spinning speeds of (a) 20 and (b) 23 kHz. Simulation parameters: $C_Q = 37.5(5)$ MHz, $\eta = 0.35(3)$, and $\delta_{iso} = -1600(10)$ ppm, $\Omega = 200(20)$ ppm, $\kappa = 0.0(1)$, $\alpha = 45(20)°$, $\beta = 0(10)°$, $\gamma = 0(10)°$.

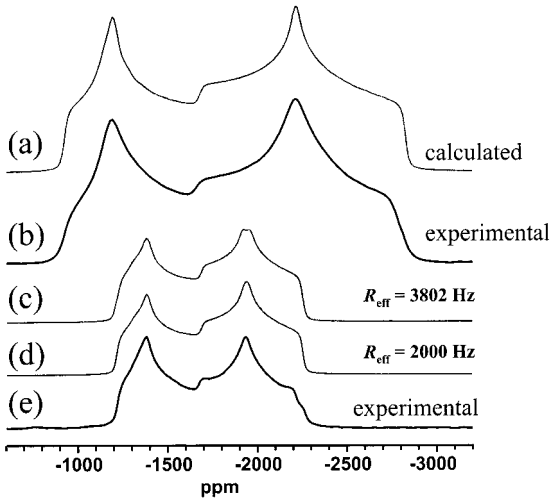

Figure 4. Experimental and simulated ^{93}Nb NMR spectra of static samples of K_2NbF_7: (a) calculated and (b) experimental spectra at 8.5 T, with ^{19}F decoupling; (c) calculated, $R_{DD}(^{93}Nb,^{19}F) = 3800$ Hz, (d) calculated, $R_{DD}(^{93}Nb,^{19}F) = 2000$ Hz, and (e) experimental spectra at 11.7 T without ^{19}F decoupling. Simulation parameters: $C_Q = 38.5(2)$ MHz, $\eta = 0.35(2)$ and $\delta_{iso} = -1600(10)$ ppm, $\Omega = 200(20)$ ppm, $\kappa = 0.0(2)$, $\alpha = 45(15)°$, $\beta = 0(5)°$, $\gamma = 0(5)°$.

overall breadth of the spectra is roughly 18 and 25 kHz at 8.5 and 11.8 T, which represents 12.5 and 20% of the total width of the two spectra, respectively. Nonetheless, careful analysis of the spectra, by, for example, varying the span of the CS tensor (Figure 5a) and the relative orientation of the CS and EFG tensors (Figure 5b), and examining the effect of this on both the static and slower spinning speed MAS spectra, gave values for Ω of 200(20) ppm and showed that the largest component of the EFG tensor, V_{33}, is coincident with the most shielded component of the CS tensor, δ_{33}.

The Hahn-echo spectra acquired at 11.7 T (Figure 4e) were acquired without ^{19}F decoupling, and thus, are expected be

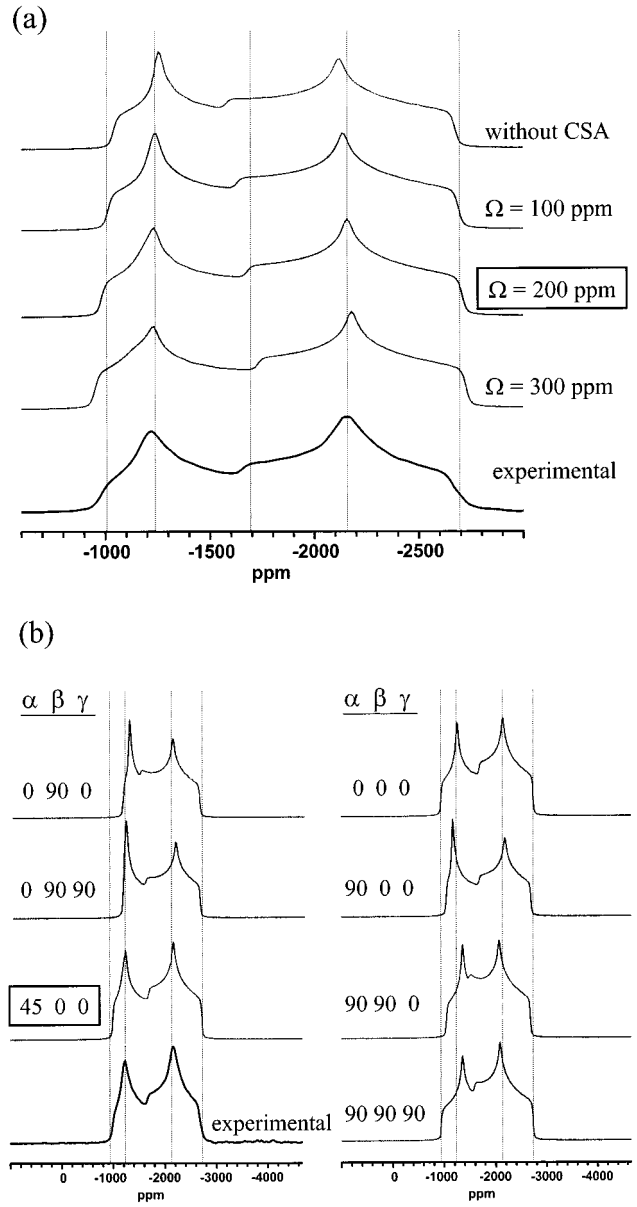

Figure 5. Experimental (black lines) and simulated (gray lines) ^{93}Nb NMR spectra of stationary samples of K_2NbF_7 acquired at 8.4 T and 60 °C. (a) The effect of changing the span of the CS tensor. (b) Effect of different relative CS and EFG tensor orientations, as defined by Euler angles α, β, and γ.

affected by the numerous ^{93}Nb, ^{19}F dipolar couplings. However, since the calculated dipolar couplings are on the order of 3.8 kHz, and may be further reduced by fluorine motion, there is not expected to be a significant effect apart from a broadening of the overall powder pattern. Nonetheless, two spectra are presented in Figures 4c and 4d, in which coupling to a single ^{19}F nucleus has been included, to show the relative size of this interaction, in comparison to the larger quadrupolar and CSA interactions. In the static ^{93}Nb spectrum acquired at 11.7 T, a small shoulder is seen in the low-frequency portion of the spectrum, which may be due to the effects of niobium−fluorine dipolar coupling.

One final point that should be addressed is the uniform excitation of the wide-line ^{93}Nb static spectra at both fields. At 11.7 T, the full spectral width is excited, with applied rf field strengths of greater than 130 kHz. However, the full spectral width of ca. 160 kHz cannot be uniformly excited at 8.5 T, as observed in the subtle differences between the intensities of the

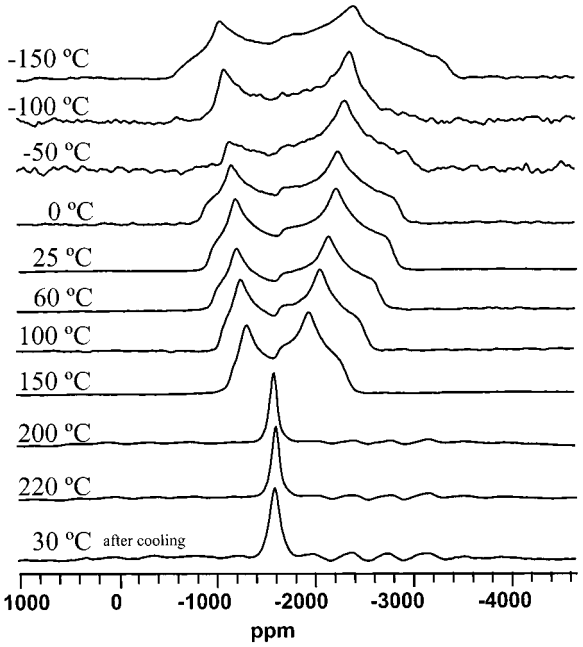

Figure 6. Variable-temperature ^{93}Nb NMR spectra of stationary samples of K_2NbF_7 acquired at 8.5 T.

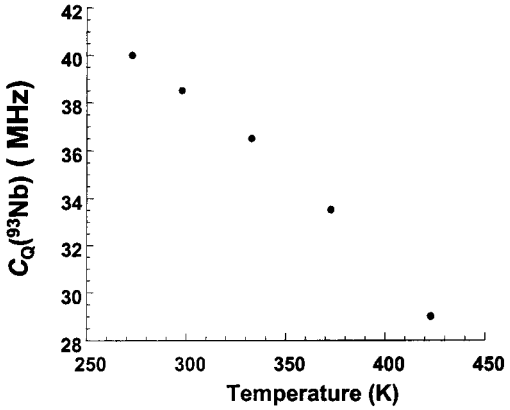

Figure 7. Plot of the variation of $C_Q(^{93}Nb)$ of K_2NbF_7 with temperature.

outer shoulders of the ^{93}Nb spectra (Figure 4a, 4b). However, there is good agreement between the experimental and calculated spectra with regard to the positions of the shoulders and discontinuities.

Variable-Temperature ^{93}Nb NMR Spectra of Stationary Samples. Variable-temperature static ^{93}Nb NMR spectra acquired at temperatures ranging from −150 to 220 °C are shown in Figure 6. It is immediately apparent that the magnitude of C_Q decreases as the temperature is increased. This is presumably associated with the intraionic motion that has been previously reported for the isostructural tantalum compound,[3] and for niobium pentahalides.[31] The motion of the fluorine atoms in NbF_7^{2-} must result in a corresponding reduction of $C_Q(^{93}Nb)$. At temperatures above 150 °C, the niobium powder pattern suddenly becomes much narrower, indicating a drastic decrease in C_Q. This is concomitant with ^{19}F and XRD data (vide infra), which indicate that a phase transition occurs at ca. 140 °C. A steady decrease in the C_Q is seen in a plot of C_Q from 0 to 140 °C (Figure 7).

Fluorine-19 MAS NMR. The ^{19}F MAS NMR spectra acquired at 8.5 and 11.7 T are shown in Figure 8. At higher spinning speeds, at both fields, nine or 10 peaks are resolved in the ^{19}F spectra, due to $^1J(^{93}Nb,^{19}F)$ coupling (since ^{93}Nb is a spin 9/2 nucleus). Unlike in solution NMR spectra, these 10

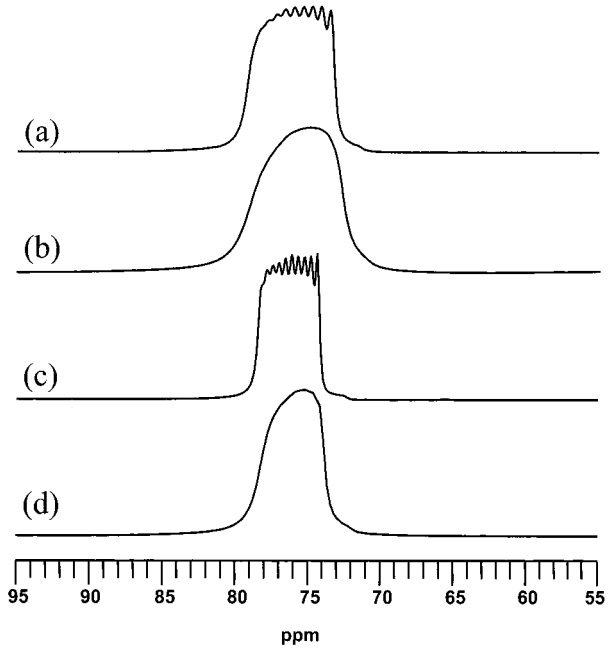

Figure 8. ^{19}F MAS NMR spectra of K_2NbF_7 acquired at (a) 8.5 T, ν_{rot} = 20 kHz, (b) 8.5 T, ν_{rot} = 10 kHz, (c) 11.7 T, ν_{rot} = 35 kHz, and (c) 11.7 T, ν_{rot} = 20 kHz.

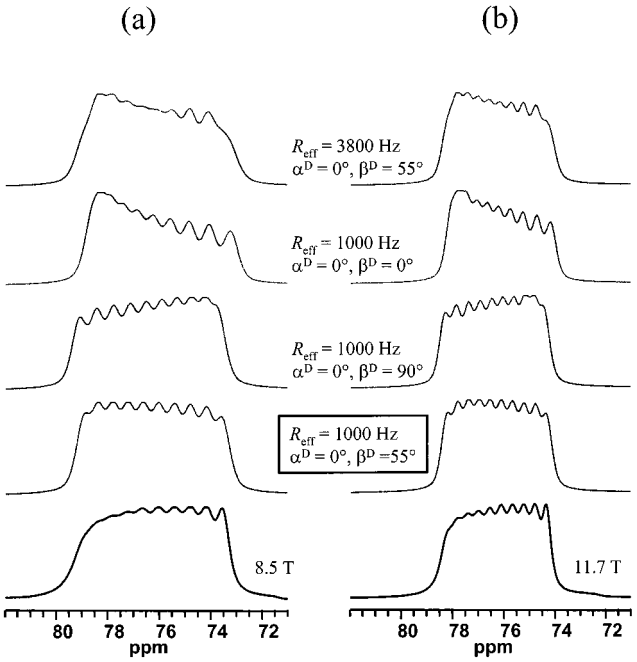

Figure 9. Experimental (black lines) and calculated (gray lines) fast-spinning ^{19}F MAS NMR spectra of K_2NbF_7 acquired at (a) 8.5 and (b) 11.7 T. The effect of changing the effective dipolar coupling, R_{eff}, and angles describing the orientation of the dipolar vector with respect to the EFG tensor, α^D and β^D, is shown. The magnitude of C_Q differs at each field due to temperature effects caused by sample spinning (i.e., (a) C_Q = 37.5 MHz, (b) C_Q = 35.5 MHz, see text for details).

peaks are not evenly spaced. The spacings between the peaks decrease slightly from low to high frequency, with some peaks broadening in this direction as well. The uneven spacing of peaks results from the presence of residual dipolar coupling between the niobium and fluorine nuclei.

Analysis of the effect of residual dipolar coupling on the ^{19}F spectra of K_2NbF_7 is nontrivial, since there are seven crystallographically inequivalent fluorine sites. It is surprising that, first, any fine structure is observed, and that, second, there appears to be a single isotropic ^{19}F chemical shift, $\delta_{iso}(^{19}F)$ = 76.3 ppm, and a single *J*-coupling of $^1J(^{93}Nb,^{19}F)$ = 204(2) Hz, despite the wide variety of bond lengths and bond angles in the NbF_7^{2-} anion. This is in agreement with previous work on the isostructural K_2TaF_7, which suggests that all the fluorine atoms rapidly exchange positions in a "floppy reorientation" process.[3] Furthermore, the presence of *J*-coupling indicates that this process does not involve long-range motion, since intermolecular exchange on the NMR time scale would eliminate the appearance of the *J*-coupling completely.

Simulations of the fast-spinning ^{19}F MAS NMR spectra were attempted using a variety of models, including a single ^{93}Nb, ^{19}F spin pair, and simulations including two, three, or four different fluorine sites with different relative EFG orientations and effective dipolar coupling constants. Quadrupolar parameters utilized in these simulations were determined from analysis of the ^{93}Nb MAS and static spectra. Not surprisingly, none of the attempted simulations closely match the experimental spectra; however, several conclusions could be drawn from these simulations. First, it is immediately apparent that simulated spectra including effective dipolar couplings on the order of 3800 Hz (determined from known Nb, F bond distances) bear little resemblance to the experimental spectra (Figure 9). The effects of residual dipolar coupling are minimal in the experimental spectra, indicating that the Nb, F dipolar coupling is likely averaged to a value on the order of 1000 ± 300 Hz, due to intraionic fluorine motion. Second, at lower spinning speeds (and therefore reduced temperatures), an increase in the asymmetry of the overall shape of the multiplet is observed (Figure 8). This indicates an increase in R_{eff}, C_Q, or both of these parameters (see eq 4). The decrease in the fluorine motion with decreasing temperature, and the corresponding effects on the ^{19}F MAS NMR spectra, are discussed in the next section of the paper. Since $^1J(^{93}Nb, ^{19}F)$ = 204(2) Hz, and reduced dipolar couplings on the order of ≤1 kHz have minimal effects of the ^{19}F MAS NMR spectra, it is expected that the anisotropy in the **J**-tensor, ΔJ, is smaller or negligible, and will not have any observable effects on the ^{19}F MAS spectra (i.e., $R_{eff} \simeq R_{DD}$).

Another unaccounted for feature of these spectra is the successive broadening of each of the transitions in the multiplet moving from low to high frequency. At this time, we have no explanation for this phenomenon, as the first-order perturbation treatment accounts only for the positions of each of the transitions in the multiplet, and not their individual broadening. In addition, careful examination of the ^{19}F MAS NMR spectra at both fields reveals a broad, low-intensity shoulder located on the low-frequency side of the multiplet. This is believed to arise from some unknown impurity in the sample, and is neglected in the remainder of the discussion.

Variable-Temperature ^{19}F MAS NMR Spectra, and X-ray Powder Diffraction Data. Fluorine-19 MAS NMR spectra acquired at low temperatures (−25 to −150 °C) and at higher temperatures (−25 to 225 °C) are shown in Figures 10a and b, respectively. Both sets of spectra are consistent with intraionic fluorine motion, as witnessed by the dramatic changes in spectral features. First, the low-temperature spectra, which were acquired at spinning speeds of 17 kHz are discussed. At ca. −50 °C, sidebands are observed, which grow in intensity as the temperature is decreased. These sideband manifolds arise from fluorine−fluorine dipolar coupling, as well as possible fluorine chemical shielding anisotropy. The increased couplings between the fluorine atoms are consistent with reduced fluorine motion at lower temperatures.

Second-moment ($<M_2>$) analysis of the static ^{19}F spectra of K_2TaF_7 and K_3ZrF_7 has previously been performed by Reyn-

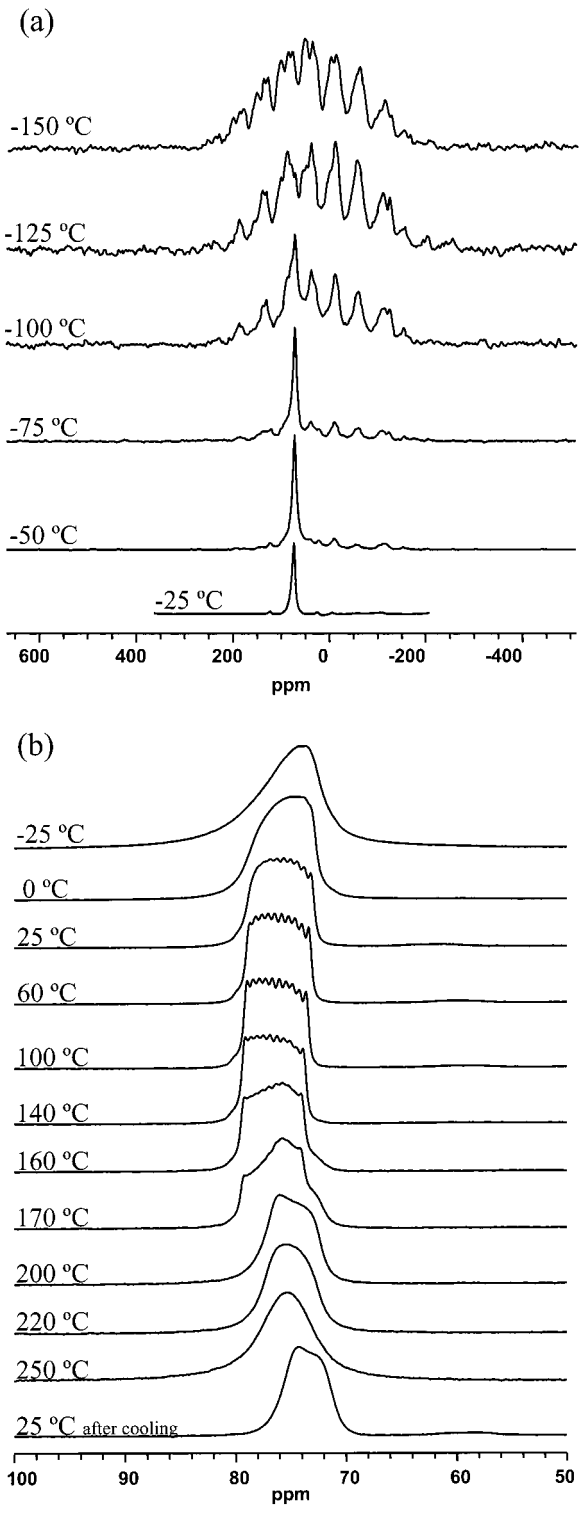

Figure 10. Variable-temperature ^{19}F MAS NMR spectra acquired at 8.5 T, temperature range from (a) −150 to −25 °C, and (b) −25 to 225 °C. The phase transition is observed at ca. 140 °C.

hardt et al. to discriminate between isotropic motion or more restricted motion involving 2-fold jumps.[3] Figure 11 shows the $<M_2>$ values for K_2NbF_7, calculated using the method outlined in reference,[32] as a function of temperature. Fluorine resonances were grouped into two kinds: one originating from rigid fluoride ions and the other originating from mobile fluoride ions, each associated with its own second moment. The second moment of the rigid ions decreases slowly when the temperature increases, decreasing from 910 to 740 kHz^2 over a temperature range of −150 to −50 °C. A resonance associated with the

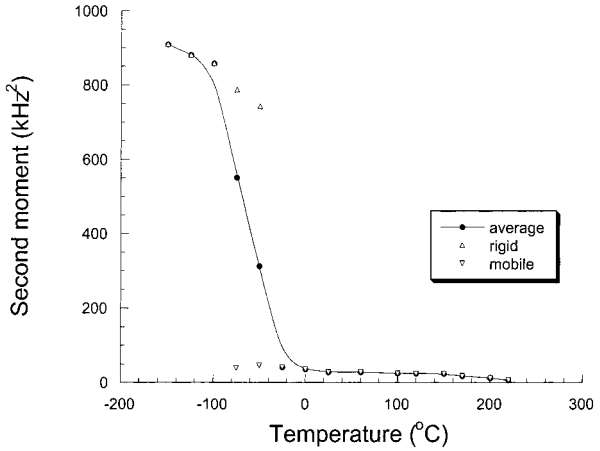

Figure 11. A plot of second moment (kHz^2) versus temperature. The second moments were calculated from the spectra in Figure 10. Fluorine resonances were grouped into two kinds: one due to rigid fluoride ions and the other due to mobile fluoride ions. The second moments of the rigid and mobile ions were calculated separately. The filled circles represent the average second moments of all fluoride ions. The second moment of the mobile ions at −100 °C is not available due to the overlap of the different resonances.

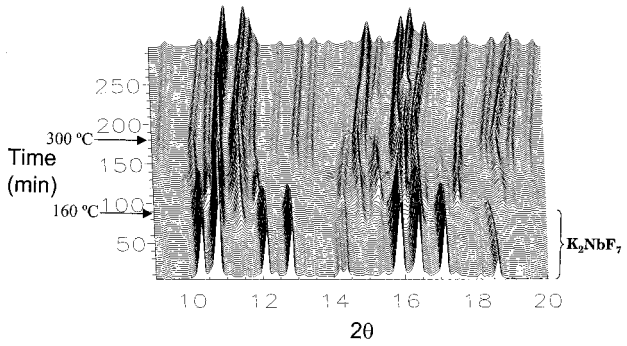

Figure 12. Time-resolved, in situ X-ray synchrotron powder diffraction patterns of K_2NbF_7 over a 5 h time period. The temperature was ramped from room temperature to 300 °C over 180 min, and was then cooled to room temperature over 120 min.

mobile ions at ca. −72 ppm is observed at −100 °C and above. The second moment of the mobile ions is less than 50 kHz^2. Some of the fluoride ions remain rigid until approximately −50 °C (Figure 10a). As in the case of K_2TaF_7, a reduction of $<M_2>$ to less than 45 kHz^2 is consistent with a rotation of the entire ion.[3] As discussed previously, the residual value of $<M_2>$ is presumably caused by interionic dipolar couplings.

Negligible sideband intensity is observed in the spectra acquired at the higher temperature range. However, the symmetry of the isotropic centerband increases with increasing temperature, again consistent with the reduction of $R_{eff}(^{93}Nb,^{19}F)$ and $C_Q(^{93}Nb)$ with increased fluorine motion at higher temperatures. At 140 to 160 °C, a distinct change in the centerband structure is observed; this is attributed to a phase transition occurring in this temperature region, which is consistent with the variable-temperature ^{93}Nb NMR data discussed earlier. No clearly-resolved *J*-couplings or residual dipolar couplings are observed in the higher temperature ^{19}F spectra, (170−250 °C), which may indicate the onset of interionic fluoride motion.

The presence of the phase transition from the known monoclinic form of K_2NbF_7 to a new crystalline phase was confirmed by time-resolved X-ray diffraction experiments (Figure 12). Small changes in both intensity and positions of the reflections were observed as the temperature was slowly ramped from room temperature, consistent with the considerable

motion observed by NMR. At ca. 160 °C (87 min) a phase change was observed and a new crystalline phase was observed. Further heating to 300 °C, resulted in significant changes in the powder pattern, especially around 130 min (225 °C); careful crystallographic analysis is required to sort out the structural changes that occur in this temperature range. These changes are not reversible: cooling the sample to room temperature resulted in the formation of yet another phase of K_2NbF_7 (n.b., a slow ramp from temperatures above 160 °C down below the phase transition results in the same NMR and XRD patterns as those recorded after fast quenching). Further work on the refinement of the structures that give rise to the high-temperature powder patterns is currently underway.

Discussion

***C*Q(93Nb).** The $C_Q(^{93}Nb)$ of 38.5(2) MHz measured at room temperature for this heptacoordinate niobium atom lies in the intermediate range of niobium quadrupole coupling constants, with very small $C_Q(^{93}Nb)$ on the order of hundreds of kHz in NbO_2F,[33] and 2.26 MHz in η^5-$C_5H_5Nb(CO)_4$,[34] larger C_Q's of 19.5 and 22 MHz in $NaNbO_3$ and $LiNbO_3$, respectively,[35,36] and very large $C_Q(^{93}Nb)$ in niobium pentahalides such as NbF_5 (between 114 and 117 MHz at 77 K),[31b] $NbCl_5$ (ca. 77 MHz, with $\eta = 0.37$ at 77 K),[31c] and $NbBr_5$ (59.71 MHz, $\eta = 0.45$ at 77 K)[31d] having been previously reported. Excluding the cyclopentadienyl complex, C_Q can be seen to increase upon moving from a cubic to pseudo-octahedral, to heptacoordinate, and finally to a pentacoordinate niobium environment.

The C_Q's of the pentahalides are extremely temperature dependent, and are observed to increase with decreasing temperature. Temperature-dependent $C_Q(^{93}Nb)$ have been previously observed in solid-state NMR experiments on $NaNbO_3$,[37] and variable-temperature NQR experiments on solid niobium pentahalides,[31] with reduction of $C_Q(^{93}Nb)$ with increasing temperature normally attributed to thermal averaging of the molecular structure. In the case of K_2NbF_7, the reduction must be due to increasing intraionic motion (e.g., vibrational motion and fluorine reorientation) which will result in rapidly changing EFG tensor axes (i.e., the orientations of these axes become averaged on the NMR time scale, as do the magnitudes of the tensor components).

CSA. Niobium-93 NMR spectra of stationary samples acquired at different magnetic field strengths reveal a small niobium CSA, and the orientation of the CS tensor with respect to the EFG tensor has been determined. Due to the relatively small contribution of the CSA to the total line width, we did not attempt to analyze the temperature dependence of the CSA. To the best of our knowledge, there is only one previous report of niobium CSA in the literature: McBrierty and co-workers[38] have proposed that there is a small CSA based on their single crystal ^{93}Nb NMR study of nonstoichiometric $LiNbO_3$. They report a difference in chemical shift of ca. 110 ppm between the crystal oriented in the field along the crystallographic *a* and *c* axes; however, the spectra are broadened due to a distribution of quadrupolar parameters, and the CS tensor is not further quantified. In addition, later single-crystal studies of $LiNbO_3$ suggested that crystal defects, which occur during crystal growth, are present, which may introduce an error into the exact determination of the niobium CSA in this sample.[39]

***J*-Coupling.** Our measured value for $^1J(^{93}Nb,^{19}F)$ for the seven-coordinated compound is smaller, as expected, than values of $^1J(^{93}Nb,^{19}F)$ which have been reported for octahedral and pentahedral niobium fluoride complexes from ^{19}F solution NMR experiments on NbF_6^- ($^1J(^{93}Nb,^{19}F) = 345$ Hz)[40] and $NbF_5 \cdot 2(CH_3)_2SO$ ($^1J(^{93}Nb,^{19}F) = 335$ Hz).[41] Note, there are no previous reports of $^1J(^{93}Nb,^{19}F)$ measured in the solid state. $^1J(^{93}Nb, ^{31}P)$ has, however, been measured in solid niobium half-sandwich complexes via solid-state ^{31}P MAS NMR experiments.[42]

Simulations. Simulations of the ^{93}Nb static and slow-spinning (20 and 23 kHz) spectra required 8 independent parameters. The availability of high-speed (and high-field MAS) spectra in which the spinning sidebands are separated from the isotropic centerband, however, allowed the C_Q and η to be obtained independently. One disadvantage of acquiring spectra under fast MAS NMR conditions, particularly relevant in our system, is the effect of sample heating due to MAS on the quadrupolar interaction. For example, in the 2.5 mm fast MAS NMR probe utilized in our experiments, the temperature inside of the rotor may be as high as 70 °C at spinning speeds on the order of 35 kHz.[43] One solution to this problem may be to use slower spinning and pulse sequences such as QPASS,[44,45] which allow for the suppression of the spinning sidebands.

Motion and Phase Transitions. A phase transition was observed by XRD at 160 °C, and by NMR, in the 3.2 mm probe, at a measured temperature of 140 °C. This measured temperature corresponds to a real temperature of 161 °C (see eq 5), thus the temperatures of the phase transitions are similar, as observed by both techniques. That the phase transition does not occur until above 150 °C in the static ^{93}Nb NMR (obtained with the 7.5 mm probe), is in agreement with other measurements.

The observation of *J*-coupling until ca. 160 °C (real temperature) indicates that motion is intraionic and not interionic in this temperature range. Two plateaus were found in the second moment analysis with values of ca. 900 and 40 kHz^2 over the temperature range of −25 to 250 °C and below −125 °C, respectively. The second moment drops rapidly between −125 and −25 °C, this temperature range clearly corresponding to the intermediate regime of fluoride-ion motion, fluoride ions existing in the slow regime below ca. −150 °C. The intermediate regime of fluorine ion motion also corresponds to the temperature range in the static ^{93}Nb NMR experiments, where poor signal-to-noise is obtained and the spectra are very difficult to simulate (see the spectra at −50 and −100 °C in Figure 6). Presumably this is a consequence of the slowly changing orientations of the EFG and CSA tensors in this regime. Finally, the high-temperature phase appears to contain considerable anionic NbF_7^{2-} and F^- motion, as witnessed by the lack of *J*-coupling and the small $C_Q(^{93}Nb)$.

Conclusion

A combination of ^{93}Nb and ^{19}F solid-state NMR experiments on spinning and stationary samples and X-ray diffraction data has provided a correlation between NMR interaction parameters, local structure and intramolecular motion. The large C_Q and nonzero asymmetry parameter are consistent with an asymmetric, heptacoordinate environment about the niobium atom. The magnitude of $C_Q(^{93}Nb)$ in the heptacoordinate niobium coordination environment is found to lie between known values of C_Q in distorted-octahedral (ca. 20 MHz) and pentacoordinate (>57 MHz) arrangements. Despite the large quadrupolar-dominated static powder patterns, a small contribution arising from anisotropic chemical shielding interactions is also observed. Fluorine-19 fast MAS NMR experiments have provided the first measurement of $^1J(^{93}Nb, ^{19}F)$ in the solid-state. The observation of $^1J(^{93}Nb, ^{19}F)$ provides clear evidence that interanionic fluoride exchange between NbF_7^{2-} anions is not occurring at ambient temperatures, but that the motion involves individual NbF_7^{2-} ions. These types of motion are sometimes extremely difficult

to distinguish definitively one from another on the basis of the shape and size of the ^{19}F sideband manifolds alone.

Variable-temperature ^{93}Nb and ^{19}F experiments provide further insight into intraionic motion, with decreasing values of C_Q and R_{DD} being observed as the temperature is increased. The observation of the phase transition at 140 °C into an unknown crystalline phase is observed by variable-temperature NMR, and is confirmed by time-resolved XRD methods. The narrow ^{93}Nb powder patterns of the new phase indicate that the niobium atoms are located in higher symmetry environments and/or that considerable motion is occurring.

Acknowledgment. We would like to thank the NSF for funding this research (DMR9901308). C.P.G. is a Cottrell Scholar of the Research Corporation. Thanks are also extended to Michael F. Ciraolo (SUNY at Stony Brook), for acquiring the XRD powder patterns. We especially thank Dr. Tony Bieleski (Bruker Instruments, Billerica, MA) for assistance in acquisition of the solid-state NMR spectra at 11.7 T, and Bruker Instruments for spectrometer time.

References and Notes

(1) Some recent examples include (a) Chamelot, P.; Lafage, B.; Taxil, P. *J. Electrochem. Soc.* **1996**, *143*, 1570. (b) Lantelme, F.; Berghoute, Y.; von Barner, J. H.; Picard, G. S. *J. Electrochem. Soc.* **1995**, *142*, 4097. (c) Alimova, Z.; Polyakov, E.; Polyakova, L.; Kremenetskii, V. *J. Fluorine Chem.* **1992**, *59*, 203.

(2) Torardi, C. C.; Brixner, L. H.; Blasse, G. *J. Solid State Chem.* **1987**, *67*, 21.

(3) (a) Reynhardt, E. C.; Pratt, J. C.; Watton, A.; Petch, H. E. *J. Phys. C: Solid State Phys.* **1981**, *14*, 4701. (b) English, R. B.; Heyns, A. M.; Reynhardt, E. C. *J. Phys. C: Solid State Phys.* **1983**, *16*, 829.

(4) Hoard, J. L. *J. Am. Chem. Soc.* **1939**, *61*, 1252.

(5) Brown, G. M.; Walker, L. A. *Acta Crystallogr.* **1966**, *20*, 220.

(6) Blaumanis, R.; Coyle, F. T. ACS Southwest Regional Meeting, Dec. 1966.

(7) Fuller, G. H. *J. Phys. Chem. Ref. Data* **1976**, *5*, 835.

(8) Baugher, J. F.; Taylor, P. C.; Oja, T.; Bray, P. J. *J. Chem. Phys.* **1969**, *50*, 4914.

(9) Taylor, P. C.; Baugher, J. F.; Kriz, H. M. *Chem. Rev.* **1975**, *75*, 203.

(10) Cheng, J. T.; Edwards, J. C.; Ellis, P. D. *J. Phys. Chem.* **1990**, *94*, 553.

(11) Power, W. P.; Wasylishen, R. E.; Mooibroek, S.; Pettitt, B. A.; Danchura, W. *J. Phys. Chem.* **1990**, *94*, 591.

(12) Koons, J. M.; Hughes, E.; Cho, H. M.; Ellis, P. D. *J. Magn. Reson. A* **1995**, *114*, 12.

(13) Zare, R. N. *Angular Momentum − Understanding Spatial Aspects in Chemistry and Physics*; John Wiley & Sons: New York, 1988.

(14) (a) Wang, F.; Grey, C. P. *J. Am. Chem. Soc.* **1995**, *117*, 6637−6638. (b) Wang, F.; Grey, C. P. *J. Am. Chem. Soc.* **1998**, *120*, 970−980.

(15) (a) Farrar, T. C.; Becker, E. D. *Pulse and Fourier Transform NMR*; Academic Press: New York, 1971. (b) Wasylishen, R. E. *Practical Spectroscopy Series*; Dybowski, C., Lichter, R. L., Eds.; Marcel Dekker: New York, 1987; Vol. 5, pp 45−91. (c) Werbelow, L. G.; Allouche, A.; Pouzard, G. *J. Chem. Soc., Faraday Trans. 2* **1987**, *83*, 871. (d) Werbelow, L. G.; London, R. E. *J. Chem. Phys.* **1995**, *102*, 5181.

(16) Harris, R. K.; Olivieri, A. C. *Prog. NMR Spectrosc.* **1992**, *24*, 435.

(17) (a) Harris, R. K. In *Encyclopedia of Nuclear Magnetic Resonance*; Grant, D. M., Harris, R. K., Eds.; John Wiley & Sons: Chichester, U.K., 1996; pp 2909−2914. (b) McDowell, C. A. In *Encyclopedia of Nuclear Magnetic Resonance*; Grant, D. M., Harris, R. K., Eds.; John Wiley & Sons: Chichester, U.K., 1996; pp 2901−2908.

(18) Grondona, P.; Olivieri, A. C. *Concepts Magn. Reson.* **1993**, *5*, 319.

(19) Olivieri, A. C.; Frydman, L.; Diaz, L. E. *J. Magn. Reson.* **1987**, *75*, 50.

(20) Apperly, D. C.; Haiping, B.; Harris, R. K. *Mol. Phys.* **1989**, *68*, 1277.

(21) Olivieri, A. C. *J. Magn. Reson.* **1989**, *81*, 201.

(22) Menger, E. M.; Veeman, W. S. *J. Magn. Reson.* **1982**, *46*, 257.

(23) Alarcón, S. H.; Olivieri, A. C.; Harris, R. K. *Solid State Nucl. Magn. Reson.* **1993**, *2*, 325.

(24) Wasylishen, R. E. *Encyclopedia of Nuclear Magnetic Resonance*; Grant, D. M., Harris, R. K., Eds.; John Wiley & Sons: Chichester, U.K., 1996; pp 1685−1695.

(25) Doty, F. D.; Ellis, P. D. *Rev. Sci. Instrum.* **1981**, *52*, 1868.

(26) Alderman, D. W.; Solum, M. S.; Grant, D. M. *J. Chem. Phys.* **1986**, *84*, 3717.

(27) (a) Eden, M.; Lee, Y. K.; Levitt, M. H. *J. Magn. Reson.* **1996**, *120*, 56. (b) Charpentier, T.; Fermon, C.; Virlet, J. *J. Magn. Reson.* **1998**, *132*, 181.

(28) Smith, S. A.; Levante, T. O.; Meier, B. H.; Ernst, R. R. *J. Magn. Reson.* **1994**, *106a*, 75−105.

(29) (a) Norby, P. *J. Am. Chem. Soc.* **1997**, *119*, 5215. (b) Norby, P. *Mater. Sci. Forum* **1996**, *147*, 229.

(30) (a) Grimmer A.-R.; Kretschmer A.; Cajipe V. B. *Magn. Reson. Chem.* **1997**, *35*, 86−90. (b) van Gorkum, L. C. M.; Hook, J. M.; Logan, M. B.; Hanna, J. V.; Wasylishen, R. E. *Magn. Reson. Chem.* **1995**, *33*, 791−795. (c) Neue, G.; Dybowski, C. *Solid State Nucl. Magn. Reson.* **1997**, *7*, 333−336.

(31) (a) Okubo, N. *J. Phys. Soc. Jpn.* **1982**, *51*, 524. (b) Okubo, N. *J. Phys. Soc. Jpn.* **1982**, *51*, 532. (c) Okubo, N. *J. Phys. Soc. Jpn.* **1982**, *51*, 1347. (d) Okubo, N.; Abe, Y. *Phys. Lett. A* **1984**, *106*, 435.

(32) Matti, M.; Waugh, J. S. *J. Chem. Phys.* **1979**, *70*, 3300.

(33) Man, P. P.; Theveneau, H.; Papon, P. *J. Magn. Reson.* **1985**, *64*, 271.

(34) Rehder, D.; Paulsen, K.; Basler, W. *J. Magn. Reson.* **1983**, *53*, 500.

(35) Meadows, M. D.; Smith, K. A.; Kinsey, R. A.; Rothgeb, T. M.; Skarjune, R. P.; Oldfield, E. *Proc. Natl. Acad. Sci. U.S.A.* **1982**, *79*, 1351.

(36) Peterson, G. E.; Bridenbaugh, P. M. *J. Chem. Phys.* **1968**, *48*, 3402.

(37) Wolf, F.; Kline, D.; Story, H. S. *J. Chem. Phys.* **1970**, *53*, 3538.

(38) Douglass, D. C.; Peterson, G. E.; McBrierty, V. J. *Phys. Rev. B* **1989**, *40*, 10694.

(39) Yatsenko, A. V.; Ivanova, E. M. *Phys. Solid State* **1995**, *37*, 1237.

(40) Hatton, J. V.; Saito, Y.; Schneider, W. G. *Can. J. Chem.* **1965**, *43*, 47.

(41) Moss, K. C. *J. Chem. Soc. (A)* **1970**, 1224.

(42) (a) Gobetto, R.; Harris, R. K.; Apperley, D. C. *J. Magn. Reson.* **1992**, *96*, 119. (b) Gibson, V. C.; Gobetto, R.; Harris, R. K.; Langdale-Brown, C.; Siemeling, U. *J. Organomet. Chem.* **1994**, *479*, 207.

(43) Langer, B.; Schnell, I.; Spiess, H. W.; Grimmer, A.-R. *J. Magn. Reson.* **1999**, *138*, 182.

(44) Massiot, D.; Montouillout, V.; Fayon, F.; Florian, P.; Bessada, C. *Chem. Phys. Lett.* **1997**, *272*, 295.

(45) Aurentz, D. J.; Vogt, F. G.; Mueller, K. T.; Benesi, A. J. *J. Magn. Reson.* **1999**, *138*, 320.